

On the dynamic efficiency of internal shocks in magnetized relativistic outflows

P. Mimica^{1*} and M. A. Aloy¹

¹*Departamento de Astronomía y Astrofísica, Universidad de Valencia, 46100, Burjassot, Spain*

17 November 2021

ABSTRACT

We study the dynamic efficiency of conversion of kinetic-to-thermal/magnetic energy of internal shocks in relativistic magnetized outflows. We model internal shocks as being caused by collisions of shells of plasma with the same energy flux and a non-zero relative velocity. The contact surface, where the interaction between the shells takes place, can break up either into two oppositely moving shocks (in the frame where the contact surface is at rest), or into a reverse shock and a forward rarefaction. We find that for moderately magnetized shocks (magnetization $\sigma \approx 0.1$), the dynamic efficiency in a single two-shell interaction can be as large as 40%. Thus, the dynamic efficiency of moderately magnetized shocks is larger than in the corresponding unmagnetized two-shell interaction. If the slower shell propagates with a sufficiently large velocity, the efficiency is only weakly dependent on its Lorentz factor. Consequently, the dynamic efficiency of shell interactions in the magnetized flow of blazars and gamma-ray bursts is effectively the same. These results are quantitatively rather independent on the equation of state of the plasma. The radiative efficiency of the process is expected to be a fraction $f_r < 1$ of the estimated dynamic one, the exact value of f_r depending on the particularities of the emission processes which radiate away the thermal or magnetic energy of the shocked states.

Key words: Hydrodynamics – (magnetohydrodynamics) MHD – Shock waves – gamma-rays: bursts – galaxies: BL Lacertae objects: general

1 INTRODUCTION

Internal shocks (Rees & Meszaros 1994) are invoked to explain the variability of blazars (see e.g., Spada et al. 2001; Mimica et al. 2005) and the light curves of the prompt phase of gamma-ray bursts (GRBs) (Sari & Piran 1995, 1997; Daigne & Mochkovitch 1998). A possible problem in this model is the question whether this mechanism is efficient enough to explain the relation between the observed energies both in the prompt GRB phase and in the afterglow (see e.g., Kobayashi et al. 1997 (KPS97), Beloborodov 2000, Kobayashi & Sari 2000, Fan & Piran 2006). To assess the efficiency of the internal shock model, most of the previous works focus on the comparison between the observed light curves and the model predictions employing a simple inelastic collision of two-point masses (KPS97; Lazzati et al. 1999; Nakar & Piran 2002; Tanihata et al. 2003; Zhang & Mészáros 2004). Less attention has been paid to the hydrodynamic effects during the shell collision (but see Kobayashi & Sari 2000; Kino et al. 2004; Mimica et al. 2004, 2005; Bošnjak et al. 2009).

The ejecta in GRBs and blazars may be rather magnetized, particularly if they are originated as a Poynting-flux-dominated flow (e.g., Usov 1992) Forming shocks in highly magnetized me-

dia is challenging (Rees & Gunn 1974; Kennel & Coroniti 1984). Therefore, to account for the observed phenomenology it is necessary to address how efficient the process of internal collisions in arbitrarily magnetized flows is. This question has been partly considered by a few recent works (e.g., Fan et al. 2004; Mimica et al. 2007).

The base to study the efficiency of internal collisions is the determination of the dynamic efficiency of a single binary collision, i.e., the efficiency of converting the kinetic energy of the colliding fluid into thermal and/or magnetic energy. Note that the radiative efficiency (i.e., the efficiency of converting the kinetic energy of the flow into radiation) is expected to be somewhat smaller. According to, e.g., Panaitescu et al. (1999) and Kumar (1999), it can be as low as $f_r \sim 0.1$. As we shall show in this paper, binary collisions in relativistic, magnetized flows can be an efficient enough way to dissipate a major fraction of the bulk kinetic energy of a relativistic ejecta. Therefore, it will depend on the efficiency of the particular radiation mechanism, that produces the observed emission (i.e., on the factor f_r), that the model of internal shocks be efficient enough to explain the observations (particularly, the distribution of energies between the prompt GRB phase and the afterglow phase).

We model internal shocks as shells of plasma with the same energy flux and a non-zero relative velocity. The contact surface, where the interaction between the shells takes place, can break up

* E-mail: Petar.Mimica@uv.es

either into two oppositely moving shocks (in the frame where the contact surface is at rest), or into a reverse shock and a forward rarefaction. The determination of whether one or the other possibility occurs is computed by estimating the invariant relative velocity between the fastest and the slowest shell, i.e., by solving the Riemann problem posed by the piecewise uniform states given by the physical quantities on the two interacting shells (Section 2). In Section 3 we define precisely the notion of dynamic efficiency, both for shocks and rarefactions. We perform a parametric study of the binary shell collision dynamic efficiency in Section 4. The discussion and conclusions are listed in Section 5. Finally, we have extended our analysis on the dynamic efficiency of internal shocks in magnetized, relativistic plasma to consider more realistic equations of state in the Appendix.

2 RELATIVISTIC MAGNETOHYDRODYNAMIC RIEMANN PROBLEM

We model the interaction between parts of the outflow with varying properties by considering Riemann problems, i.e. relativistic magnetohydrodynamic initial-value problems with two constant states separated by a discontinuity in planar symmetry. We note, that we could use a more sophisticated approach consisting on performing numerical relativistic magnetohydrodynamic (RMHD) simulations of the interaction of parts of the outflow with different velocities. However, such an approach demands huge computational resources (even performing one dimensional simulations using the same code as in Mimica et al. 2009), and we are interested in sampling very finely a large parameter space with our models. Apart from this numerical reason, it is in order to point out that, by the internal shock phase, the lateral expansion of the flow is very small, since the flow is probably cold and ultrarelativistic. Thus, a description of the interactions assuming planar symmetry suffices to compute the dynamic efficiency of such interactions (rather than a more complex spherically symmetric approach).

In the following we use subscripts L and R to denote properties of the (faster) left and (slower) right state, respectively. To avoid repeated writing of a factor 4π and the speed of light c , we normalize the rest-mass density ρ to ρ_R , the energy density to $\rho_R c^2$ and the magnetic field strength to $c\sqrt{4\pi\rho_R}$.

2.1 Initial states of the Riemann problem

For the initial thermal pressure of both states we assume that it is small fraction of the density, $p_L = \chi\rho_L$ and $p_R = \chi$. We assume magnetic fields perpendicular to the direction of the flow propagation. The remaining parameters determining the RMHD Riemann problem are: the density contrast ρ_L , the Lorentz factor of the right state Γ_R , the relative Lorentz factor difference $\Delta g := (\Gamma_L - \Gamma_R)/\Gamma_R$, and the magnetizations of left and right states, $\sigma_L := B_L^2/(\Gamma_R^2(1 + \Delta g)^2\rho_L)$ and $\sigma_R := B_R^2/\Gamma_R^2$, where B_L and B_R are the lab frame magnetic field strengths of left and right states, respectively. Furthermore, we define the total (thermal + magnetic) pressure

$$p^* := p + \frac{B^2}{2\Gamma^2} = p + \frac{\sigma\rho}{2}, \quad (1)$$

the total specific enthalpy

$$h^* := 1 + \epsilon + p/\rho + \sigma, \quad (2)$$

and

$$e^* := \rho(1 + \epsilon) + \frac{\sigma\rho}{2}. \quad (3)$$

where ϵ denotes the specific internal energy and is dependant on the equation of state used (see Section 3.1).

The general solution of a RMHD Riemann problem was found by Giacomazzo & Rezzolla (2006), and recently used in RMHD numerical codes by e.g., van der Holst et al. (2008). However, here we deal with a degenerate RMHD configuration, which solution was first found by Romero et al. (2005). The typical structure of the flow after the break up of the initial discontinuity consists of two initial states, and two intermediate states separated by a contact discontinuity (CD). The total pressure and velocity are the same on both sides of the CD. The quantity σ/ρ is uniform everywhere, except across the CD, where it can have a jump. We denote the total pressure of intermediate states p_S^* , and rest-mass density left and right of the CD as $\rho_{S,L}$ and $\rho_{S,R}$. In the context of internal shocks, if the flow is ultrarelativistic in the direction of propagation, the velocity components perpendicular to the flow propagation should be negligibly small and, hence, they are set up to zero in our model¹.

2.2 Conditions for the existence of a two-shock solution

One of the key steps in solving a Riemann problem is to determine under which conditions internal shocks can form. States ahead and behind the shock front are related by the Lichnerowicz adiabat (Romero et al. 2005)

$$(h_b^*)^2 - (h_a^*)^2 - \left(\frac{h_b^*}{\rho_b} - \frac{h_a^*}{\rho_a} \right) (p_b^* - p_a^*) = 0. \quad (4)$$

Following Rezzolla & Zanotti (2001), we study the relative velocity between the states ahead (a) and behind (b) the shock front (all velocities are measured in the rest frame of the shock, and all thermodynamic properties are measured in the fluid rest frame),

$$v_{ab} := \frac{v_a - v_b}{1 - v_a v_b} = \sqrt{\frac{(p_b^* - p_a^*)(e_b^* - e_a^*)}{(e_a^* + p_b^*)(e_b^* + p_a^*)}}. \quad (5)$$

In our case states ahead of the shock are the initial (L, R) states, while states behind the shock are the intermediate states. Since v_{ab} is Lorentz-invariant, we can measure the velocity ahead of the left-propagating (*reverse*) shock (RS) in the frame in which the CD is at rest,

$$v_l = \sqrt{\frac{(p_S^* - p_L^*)(e_{S,L}^*(p_S^*) - e_L^*)}{(e_L^* + p_S^*)(e_{S,L}^*(p_S^*) + p_L^*)}}. \quad (6)$$

Likewise, the velocity ahead of the right-going (*forward*) shock (FS) measured in the CD frame is

$$v_r = -\sqrt{\frac{(p_S^* - p_R^*)(e_{S,R}^*(p_S^*) - e_R^*)}{(e_R^* + p_S^*)(e_{S,R}^*(p_S^*) + p_R^*)}}. \quad (7)$$

where $e_{S,L}^*$ and $e_{S,R}^*$ are the energy densities of the states to the left and to the right of the CD, respectively. The rest-mass densities $\rho_{S,L}$ and $\rho_{S,R}$ can be obtained from (4) and (2).

Since both FS and RS only exist if $p_S^* > p_R^*$ and $p_S^* > p_L^*$, respectively, with decreasing p_S^* either the FS will disappear first (for $p_S^* = p_R^* > p_L^*$, giving $v_r = 0$) or the RS will disappear first (for $p_S^* = p_L^* > p_R^*$, giving $v_l = 0$). Using equations (6) and (7) and the

¹ If such velocities were significant, appreciable changes in the Riemann structure may result as pointed out in Aloy & Rezzolla (2006) or Aloy & Mimica (2008).

invariance of the relative velocity between the left and right states, $v_{lr} := (v_l - v_r)/(1 - v_l v_r)$, we can determine the minimum relative velocity for which a two-shock solution is possible

$$(v_{lr})_{2S} = \begin{cases} \sqrt{\frac{(p_L^* - p_R^*)(e_{S,R}^*(p_L^*) - e_R^*)}{(e_{S,R}^*(p_L^*) + p_R^*)(e_R^* + p_L^*)}} & \text{if } p_L^* = p_S^* > p_R^* \\ \sqrt{\frac{(p_R^* - p_L^*)(e_{S,L}^*(p_R^*) - e_L^*)}{(e_{S,L}^*(p_R^*) + p_L^*)(e_L^* + p_R^*)}} & \text{if } p_L^* < p_R^* = p_S^* \end{cases} \quad (8)$$

Generally, the quantity $(v_{lr})_{2S}$ can be only determined numerically. If $(v_{lr}) < (v_{lr})_{2S}$, a single shock and a rarefaction emerge from the initial discontinuity. It is even possible that instead of two shocks two rarefactions form (see, Rezzolla & Zanotti 2001).

3 ENERGY DISSIPATION EFFICIENCY OF INTERNAL SHOCKS

Internal shocks in relativistic outflows are invoked as moderately efficient means of conversion of the kinetic energy of the flow into radiation. In this section we present our model for inhomogeneous, ultrarelativistic outflows and provide an operative definition for the efficiency of conversion of the initial energy of the outflow into thermal and magnetic energy produced by internal shocks. We assume that a fraction of this thermal and magnetic energy will be radiated away.

3.1 Outflow model

To study internal shocks we idealize interactions of parts of the outflow moving with different velocities as collisions of homogeneous shells. In our model the faster (left) shell catches up with the slower (right) one yielding, in some cases, a pair of shocks propagating in opposite directions (as seen from the CD frame). In order to cover a wide range of possible flow Lorentz factors and shell magnetizations, we assume that initially, the flux of energy in the lab frame is uniform and the same in both shells². The energy flux for a shell with rest-mass density ρ , ratio of thermal pressure to density χ , magnetization σ and Lorentz factor Γ is (e.g., Leismann et al. 2005).

$$F_\tau := \rho \left[\Gamma^2 (1 + \epsilon + \chi + \sigma) - \Gamma \right] \sqrt{1 - \Gamma^{-2}}. \quad (9)$$

Using the notation introduced in Section 2.1 and assuming the equality of F_τ in both shells we find that the density contrast ρ_L between left and right shells is

$$\rho_L = \frac{(1 + \Delta g)^{-2} \left[1 + \epsilon + \chi + \sigma_R - \Gamma_R^{-1} \right] \sqrt{1 - \Gamma_R^{-2}}}{\left[1 + \epsilon + \chi + \sigma_L - \Gamma_R^{-1} (1 + \Delta g)^{-1} \right] \sqrt{1 - \Gamma_R^{-2} (1 + \Delta g)^{-2}}}. \quad (10)$$

Considering σ_L , σ_R , Γ_R and Δg as parameters, we can use (10) to compute the rest of the variables needed to set-up the Riemann problem. We then compute the break up of the initial discontinuity between both shells using the exact Riemann solver developed by Romero et al. (2005).

In the following we use a polytropic equation of state with an adiabatic index $\hat{\gamma} = 4/3$:

² In Mimica et al. (2009) we use a similar model to compare afterglow ejecta shells with different levels of magnetization, with a slight difference that in that study, instead of having the same flux of energy, all the ejecta shells were assumed to contain the same total energy.

$$\epsilon := \frac{p}{(\hat{\gamma} - 1)\rho} \quad (11)$$

As we show in the Appendix, the Riemann solver of Romero et al. (2005) has been suitably modified to include a more realistic equation of state. However, we find no qualitative differences between the results using a polytropic EoS (with either $\hat{\gamma} = 4/3$ or $\hat{\gamma} = 5/3$) and $\hat{\gamma}$ -variable EoS. Furthermore, the quantitative differences are very small in terms of dynamic efficiency.

3.2 Efficiency of energy dissipation by a shock

To model the dynamic efficiency of energy dissipation we follow the approach described in Mimica et al. (2007), suitably modified to account for the fact that in the present work, there can occur situations where either the FS or the RS do not exist (see Section 2.2). By using the exact solver we determine the existence of shocks and (in case one or two shocks exist) obtain the hydrodynamic state of the shocked fluid. We use subscripts S, L and S, R to denote shocked portions of left and right shells, respectively. In the following we treat the efficiency of each shock separately.

3.2.1 Reverse shock

To compute the efficiency we need to compare the energy content of the initial (unshocked) faster shell with that of the shocked shell at the moment when RS has crossed the initial shell. Assuming an initial shell width Δx , we define total initial kinetic, thermal and magnetic energy (see also equations (A.1) - (A.3) of Mimica et al. 2007)

$$\begin{aligned} E_K(\Gamma, \rho, \Delta x) &:= \Gamma(\Gamma - 1)\rho\Delta x \\ E_T(\Gamma, \rho, p, \Delta x) &:= [(\rho\epsilon + p)\Gamma^2 - p]\Delta x \\ E_M(\Gamma, \rho, \sigma, \Delta x) &:= \left(\Gamma^2 - \frac{1}{2} \right) \rho\sigma\Delta x \end{aligned} \quad (12)$$

When the RS crosses the whole initial shell, the length of the compressed shell (i.e., the fluid between the RS and the CD) is $\zeta_L \Delta x$, where

$$\zeta_L := \frac{v_{CD} - v_{S,L}}{v_L - v_{S,L}} < 1$$

and v_{CD} and $v_{S,L}$ are velocities (in the lab frame) of the contact discontinuity and the RS, both obtained from the solver. Without loss of generality, we can normalize the initial shell width so that $\Delta x = 1$. Then we define the dynamic *thermal* efficiency

$$\epsilon_{T,L} := \frac{E_T(\Gamma_{S,L}, \rho_{S,L}, p_{S,L}, \zeta_L) - E_T(\Gamma_R(1 + \Delta g), \rho_L, \chi\rho_L, 1)}{E_0}, \quad (13)$$

and the dynamic *magnetic* efficiency

$$\epsilon_{M,L} := \frac{E_M(\Gamma_{S,L}, \rho_{S,L}, \sigma_{S,L}, \zeta_L) - E_M(\Gamma_R(1 + \Delta g), \rho_L, \sigma_L, 1)}{E_0}, \quad (14)$$

where E_0 is the total initial energy of both shells

$$\begin{aligned} E_0 &:= E_K(\Gamma_R(1 + \Delta g), \rho_L, 1) + E_T(\Gamma_R(1 + \Delta g), \rho_L, \chi\rho_L, 1) \\ &\quad + E_M(\Gamma_R(1 + \Delta g), \rho_L, \sigma_L, 1) + E_K(\Gamma_R, 1, 1) \\ &\quad + E_T(\Gamma_R, 1, \chi, 1) + E_M(\Gamma_R, 1, \sigma_R, 1). \end{aligned} \quad (15)$$

Equations (13) and (14) express the fraction of the initial energy that the RS has converted into thermal and magnetic energy, respectively.

3.2.2 *Forward shock*

In complete analogy, we define the thermal and magnetic efficiencies for the forward shock,

$$\varepsilon_{T,R} := \frac{E_T(\Gamma_{S,R}, \rho_{S,R}, p_{S,R}, \zeta_R) - E_T(\Gamma_R, 1, \chi, 1)}{E_0}, \quad (16)$$

$$\varepsilon_{M,R} := \frac{E_M(\Gamma_{S,R}, \rho_{S,R}, \sigma_{S,R}, \zeta_R) - E_M(\Gamma_R, 1, \sigma_R, 1)}{E_0}, \quad (17)$$

where

$$\zeta_R := \frac{v_{S,R} - v_{CD}}{v_{S,R} - v_R} < 1.$$

$v_{S,R}$ is the velocity of the FS in the lab frame. Here we set $\varepsilon_{T,R} = \varepsilon_{M,R} = 0$ if the forward shock is absent.

Combining equations (13), (14), (16) and (17) we define the dynamic thermal and magnetic efficiency of internal shocks

$$\varepsilon_T := \varepsilon_{T,L} + \varepsilon_{T,R} \quad (18)$$

$$\varepsilon_M := \varepsilon_{M,L} + \varepsilon_{M,R}. \quad (19)$$

We point out that these definitions of efficiency generalize the ones typically used when cold, unmagnetized shell collisions are considered. In that case, initially one only has bulk kinetic energy in the shells (i.e., $E_0 = E_K(\Gamma_L, \rho_L, 1) + E_K(\Gamma_R, 1, 1)$). In case of collisions of arbitrarily magnetized shells with arbitrarily initial thermal content, E_0 can be substantially larger than the initial kinetic energy in the shells.

3.3 *Efficiency of energy dissipation by a rarefaction*

In a rarefaction there is a net conversion of magnetic and/or thermal energy into kinetic energy, thus the net dynamic efficiency produced by a rarefaction, defined as in e.g., Eq. (14), should be negative. The consequence of this is that, when we obtain a shock-contact-rarefaction or rarefaction-contact-shock structure as a solution to the Riemann problem, it may happen that the total (left plus right) thermal or magnetic efficiency (Eqs. (18)-(19)) was negative. However, this situation does not correctly model the fact that, in cases where a shock exists only in one of the shells, it is still able to radiate away part of the thermal or magnetic energy behind it, even though there is a rarefaction propagating through the other shell. We also point out that rarefactions happen in our case, where we model initially cold flows, as a result of a net conversion of magnetic into kinetic energy. This kinetic energy can be further recycled by the flow, and dissipated in the course of ulterior binary collisions. Therefore, directly summing the (positive) dynamic efficiency of conversion of kinetic-to-thermal/magnetic energy in a shock to the (negative) dynamic efficiency of conversion in a rarefaction is inadequate. The total dynamic efficiency in a case where only one shock forms will be determined only by the efficiency in the shocked shell. Thus, we set $\varepsilon_{T,L} = \varepsilon_{M,L} = 0$ ($\varepsilon_{T,R} = \varepsilon_{M,R} = 0$) if the reverse (forward) shock is absent. We note that this contrasts with previous works on internal collisions of unmagnetized shells (e.g., Kino et al. 2004), and may yield higher values of the net dynamic efficiency.

4 **PARAMETRIC STUDY OF THE DYNAMIC DISSIPATION EFFICIENCY**

Next we study the dynamic dissipation efficiency in the process of collision of cold, magnetized shells. The shells are assumed to

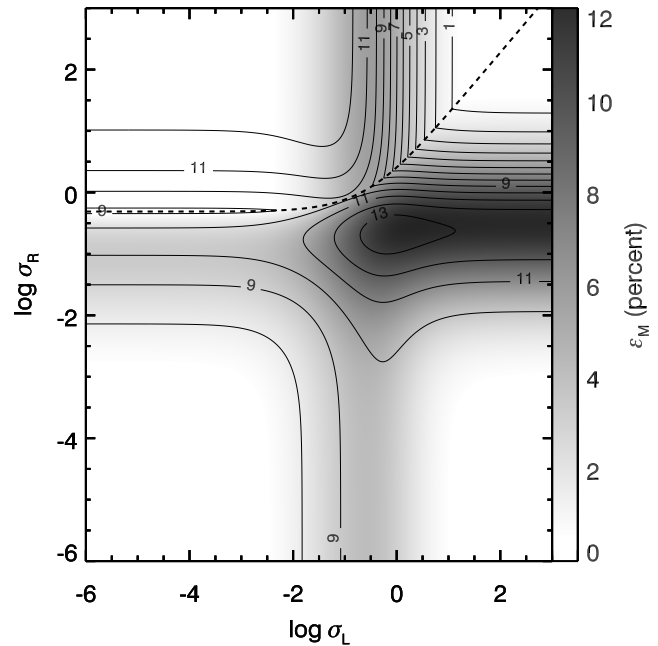


Figure 1. Contours: total dynamic efficiency $\varepsilon_T + \varepsilon_M$ (eqs. (18) and (19)) in the blazar regime ($\Gamma_R = 10$, $\Delta g = 1$) for different combinations of (σ_L, σ_R) . Contours indicate the efficiency in percent and their levels are 1, 2, 3, 4, 5, 6, 7, 8, 9, 10, 11, 12 and 13. In the region of the parameter space above the dashed line there is no forward shock, while the reverse shock is always present for the considered parametrization. Filled contours: magnetic efficiency ε_M in percent.

be cold because in the standard fireball model (e.g., Piran 2005), almost all the internal energy of the ejecta has been converted to kinetic energy *before* internal shocks start to show up. Thus, a regime where the parameter χ is large does not properly model an efficiently accelerated ejecta by non-magnetic processes. On the other hand, if the ejecta were accelerated by magnetic fields (like in Poynting-dominated flow models; e.g., Usov 1992), then the flow is cold all the way from the beginning to the internal shock phase, and then χ should also be small in such a case.

For all the models in this paper, in order to reduce the dimensions of the parameter space, we fix $\chi = 10^{-4}$ uniform everywhere, to model initially cold shells and, unless otherwise specified, set $\Delta g = 1$ as a reference value. We choose χ sufficiently small so that it does not influence the solution of the Riemann problem. In the first two subsections we consider blazar and GRB regimes. Then, we study the flow structure for three representative Riemann problems, and end the section with a discussion of the impact of varying Δg on the efficiency.

4.1 **Blazar regime**

In the blazar regime we set $\Gamma_R = 10$ as a typical value of the Lorentz factor of the outflowing material. We continuously vary σ_L and σ_R and show contours of total efficiency ($\varepsilon_T + \varepsilon_M$) in Fig. 1.

The maximum efficiency is attained for moderately magnetized slower shells ($\sigma_R \approx 0.2$) and highly magnetized left shells ($\sigma_L \approx 1$). The broad region to the right of the efficiency maximum is independent of σ_L because in a collision with such a highly magnetized fast shell almost all the energy is dissipated by the FS. In the region above the dashed line of Fig. 1 the FS is absent and, thus, since only the RS dissipates the initial energy, the efficiency

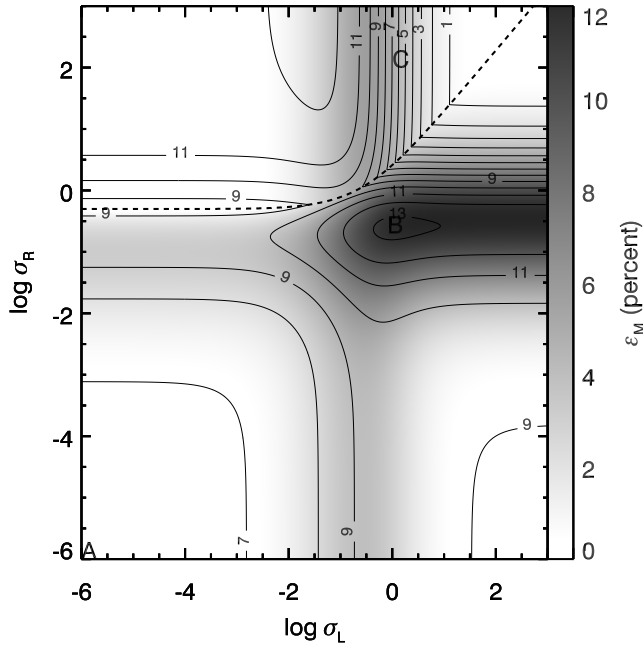


Figure 2. Same as Fig. 1, but in the GRB regime ($\Gamma_R = 100$, $\Delta g = 1$).

slightly drops. However, the transition between the regime where the two shocks operate or only the RS exists is smooth. The reason being that the efficiency below the separatrix of the two regimes and close to it is dominated by the contribution of RS.

As expected, when either σ_L or σ_R approach low values, the dynamic efficiency ceases to depend on them. This can be seen in the center of the left side of Fig. 1 where, for $\sigma_L \ll 1$, the dynamic efficiency only depends on σ_R . The converse is true in the center of the lower side of the figure, where $\sigma_R \ll 1$.

4.2 GRB regime

The results in the GRB regime ($\Gamma_R = 100$, $\Delta g = 1$) are shown in Fig. 2. The general shape of the contours is similar to Fig. 1, which is expected since both in the blazar and in the GRB regime the flow is ultrarelativistic and most of the quantities which depend on the *relative* velocity between the faster and the slower shell depend only weakly on Γ_R , Δg being the crucial parameter (Daigne & Mochkovitch 1998). For example, the dashed curve which delimits regions with and without a forward shock does not depend on Γ_R but only on Δg .

The maximum of the dynamic efficiency in the GRB regime is localized at roughly the same spot as in the blazar regime. However, compared to the former case the region of maximum efficiency (i.e., where $\varepsilon_T + \varepsilon_M \gtrsim 0.13$) is smaller.

4.3 Flow structure

In this subsection we study the flow structure for three representative models in the GRB regime. Their location in the parameter space is marked by letters *A*, *B* and *C* in Fig. 2. Model *A* corresponds to a prototype of interaction between non-magnetized shells ($\sigma_L = \sigma_R = 10^{-6}$). Model *B* is picked up to illustrate the flow structure at the maximum efficiency ($\sigma_L = 0.8$, $\sigma_R = 0.2$). Finally, model *C* corresponds to the case when the FS is absent ($\sigma_L = 1$, $\sigma_R = 10^2$). We show the rest mass density profile of these

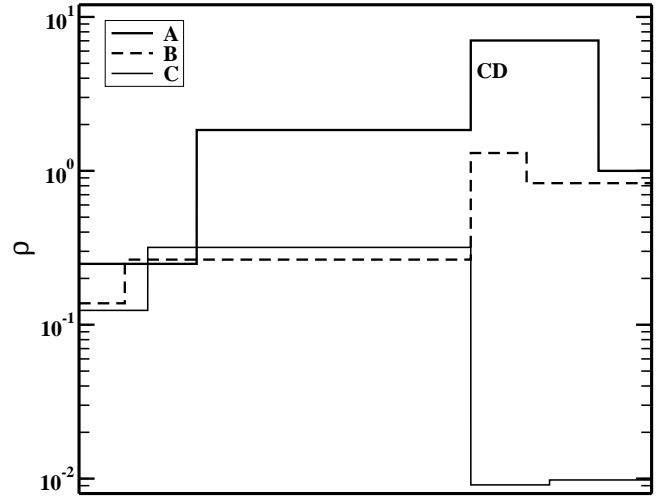


Figure 3. Rest-mass density profile of models *A*, *B* and *C* (see legends) whose parameters are given in Sect. 4.3. Profiles have been shifted so that the CD for all models coincides. In models *A* and *B* the FS and the RS are clearly visible, while in the model *C* a rarefaction wave is visible as a small “step” to the right of the CD.

models in Fig. 3. Model *A* (thick full line on Fig. 3) shows two strong shocks which dissipate kinetic into thermal energy. In contrast, model *B* (dashed line) has much weaker shocks due to non-negligible magnetization in both shells. Finally, model *C* (thin full line) does not have forward shock due to very high magnetization in the slower shell.

All three models have a substantial dynamic efficiency, but there is a qualitative difference among them. In model *A* internal shocks dissipate kinetic to thermal energy only (thermal efficiency). In model *B* shocks mainly compress the magnetic field (magnetic efficiency) and dissipate only a minor fraction of the initial kinetic and magnetic energy to thermal energy. Finally, in the model *C* only the reverse shock is active, compressing the faster shell magnetic field.

4.4 Dependence on Δg and on Δs

The choice of a relatively small value of Δg in the previous section is motivated by the results of numerical simulations of relativistic outflows (e.g Aloy et al. 2000, 2005; Mizuta et al. 2006; Zhang et al. 2003, 2004; Morsony et al. 2007; Lazzati et al. 2009; Mizuta & Aloy 2009) where $\Delta g < 2$ between adjacent parts of the flow that may catch up (but see, e.g., Kino & Takahara 2008, who find $\Delta g \sim 1 - 19$ appropriate to model Mrk 421). This adjacent flow regions can be assimilated to pairs of shells whose binary collision we are considering here.

However, it has been confirmed by several independent works (KPS97; Beloborodov 2000; Kobayashi & Sari 2000; Kino et al. 2004, etc.) that, in order to achieve a high efficiency (more than a few percent) in internal collisions of unmagnetized shells, the ratio between the maximum (Γ_{\max}) and the minimum (Γ_{\min}) Lorentz factor of the distribution of initial shells should be $\Gamma_{\max}/\Gamma_{\min} > 10$.

In view of these results, we have also made an extensive analysis of the dependence of the dynamic efficiency on the variation of Δg . Since we are also interested in evaluating the influence of the magnetic fields on the results, we define a new variable

$$\Delta s = \frac{1 + \sigma_L}{1 + \sigma_R}, \quad (20)$$

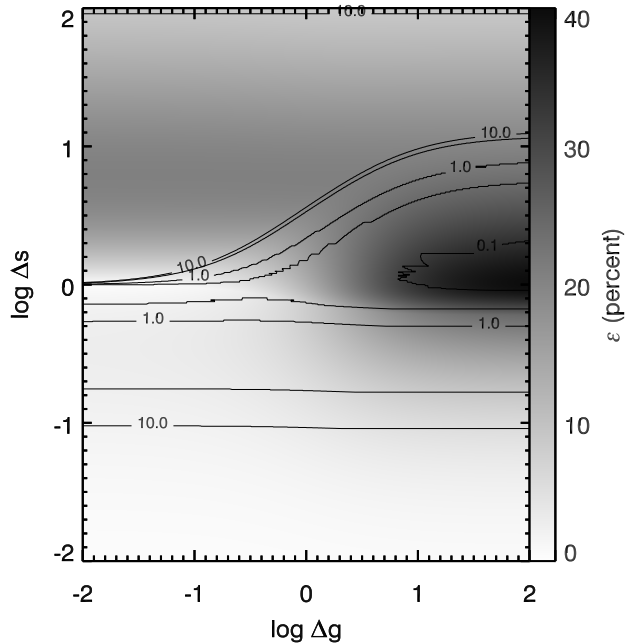


Figure 4. The gray scale indicates the value of the maximum total dynamic efficiency (in percent) as a function of the parameter pair $(\Delta g, \Delta s)$. The values of the rest of the parameters are fixed to $\Gamma_R = 100$, and $\chi = 10^{-4}$. Contours: magnetization of the slowest shell: $\sigma_R = 0.1, 0.5, 1, 5$ and 10 .

and plot (Fig. 4) the value of the maximum efficiency reached for every combination $(\Delta g, \Delta s)$ and fixed values of the rest of the parameters to $\Gamma_R = 100$, and $\chi = 10^{-4}$. To be more precise, for fixed Δg and Δs we need to look for the maximum of the efficiency of all models whose σ_L and σ_R satisfy Eq. (20). It is evident from Fig. 4 that the maximum total dynamic efficiency grows (non-monotonically) with increasing Δg , in agreement with the above mentioned works (where unmagnetized collisions have been considered). Indeed, a large value $\Delta g \gtrsim 10$ yields dynamic efficiency values $\sim 40\%$ if both shells are moderately magnetized ($\sigma_R \sim \sigma_L \lesssim 0.1$). Nevertheless, the amount of increase of efficiency with Δg depends strongly on Δs . For $|\Delta s| \gtrsim 1$, corresponding to cases where the slower shell is highly magnetized ($\sigma_R \gtrsim 4$), the maximum dynamic efficiency is almost independent of Δg ; while for $|\Delta s| \lesssim 1$, the maximum dynamic efficiency displays a strong, non-monotonic dependence on Δg .

It is remarkable that values $5 \lesssim \Delta s \lesssim 100$ yield dynamic efficiencies in excess of $\sim 20\%$, regardless of the relative Lorentz factor between the two shells. In this region of the parameter space the maximal dynamic efficiency happens when both shells are magnetized ($\sigma_R > 10$, $\sigma_L > 50$), and the total dynamic magnetic efficiency dominates the total dynamic efficiency.

5 DISCUSSION

We have focused in this paper on the estimation of the dynamic efficiency of conversion of kinetic-to-thermal/magnetic energy in collisions (internal shocks) of magnetized shells in relativistic outflows. A fundamental difference between the internal collisions in magnetized and unmagnetized outflows is the fact that in the former case not only shocks but also rarefactions can form. Thus, one would naturally expect a reduced dynamic efficiency in the magnetized case. However, we have shown that such dynamic efficiency

may reach values $\sim 10\% - 40\%$, in a wide range of the parameter space typical for relativistic outflows of astrophysical interest (blazars and GRBs). Thus, the dynamic efficiency of moderately magnetized shell interactions is larger than in the corresponding unmagnetized case. This is because when the shells are moderately magnetized, most of the initial shell kinetic energy is converted to magnetic energy, rather than to thermal energy.

The difference in efficiency between flows with moderate Lorentz factors ($\Gamma_R = 10$) and ultrarelativistic ones ($\Gamma_R = 100$) is very small, because in the ultrarelativistic kinematic limit (i.e., $\Gamma \gg 1$), once the energy flux and the magnetizations of both shells are fixed, the key parameter governing the dynamic efficiency is Δg rather than Γ_R . From numerical simulations one expects that any efficiently accelerated outflow will not display huge variations in the velocity between adjacent regions of flow. Therefore, values of $\Delta g \approx 1$ seem reasonable and $\Delta g = 1$ has been taken as a typical value for both blazars and GRB jets. A fixed value of $\Delta g = 1$ brings maximum efficiency when the magnetizations of the colliding shells are $(\sigma_L, \sigma_R) \approx (1, 0.2)$. Larger dynamic efficiency values $\sim 40\%$ are reached by magnetized internal shocks if $\Delta g \gtrsim 10$ and $|\Delta s| \lesssim 1$, corresponding to cases where the magnetization of both shells is moderate ($\sigma_R \approx \sigma_L \lesssim 0.1$).

Consistent with our previous work (Mimica et al. 2007), in the limit of low magnetization of both shells, the kinetic energy is mostly converted into thermal energy, where the increased magnetic energy in the shocked plasma is only a minor contribution to the total dynamic efficiency, i.e., $\varepsilon_T \ll \varepsilon_M$. Here we find that as the magnetization of the shells grows, the roles of ε_T and ε_M are exchanged, so that $\varepsilon_T < \varepsilon_M$ (at the maximum dynamic efficiency $\varepsilon_T \approx 0.1\varepsilon_M$). If the magnetization of both shells is large, the dynamic efficiency decreases again because producing shocks in highly magnetized media is very difficult. All these conclusions are independent on the EoS used to model the plasma, i.e., they are both qualitatively and quantitatively basically the same independent on whether a polytropic EoS with a fixed adiabatic index is taken (either $\hat{\gamma} = 4/3$ or $\hat{\gamma} = 5/3$) or a more general, analytic approximation to the exact relativistic EoS (the *TM* EoS; see Appendix) is considered.

The comparison of our results with previous analytic or semi-analytic works (e.g., KPS97; Beloborodov 2000; Kobayashi & Sari 2001; Kobayashi et al. 2002) is not straightforward. Generally, these works compute the efficiency of the collision of shells without computing their (magneto-)hydrodynamic evolution and, on the other hand, these works include not only a single collision, but the multiple interactions of a number of dense shells. The bottom line in these previous works is that internal collisions of unmagnetized shells can be extremely efficient; the efficiency exceeding 40%, or even $\sim 100\%$ (Beloborodov 2000) if the spread of the Lorentz factor (i.e., the ratio between the Lorentz factor of the faster, Γ_{\max} , and of the slower Γ_{\min} shell in the sample) is large ($\Gamma_{\max}/\Gamma_{\min} = 10^3$; e.g., KPS97, Kobayashi et al. 2002). For a more moderate spread of the Lorentz factor $\Gamma_{\max}/\Gamma_{\min} = 10$, the efficiency is $\sim 20\%$. We note that these high efficiencies are reached because a large number of binary collisions is included in the model (not only a single one as in our case). Thus, the kinetic energy which is not dissipated in the first generation of collisions (between the initially set up shells), can be further converted into internal energy as subsequent generations of collisions take place. In contrast, we find that moderate magnetizations of both shells ($\sigma \lesssim 0.1$) and $\Delta g \gtrsim 10$ (which would roughly correspond to $\Gamma_{\max}/\Gamma_{\min} = 9$) are enough for a single binary collision to reach a total dynamic efficiency of $\sim 40\%$.

We point out that the energy radiated in the collision of magne-

tized shells is only a fraction, $f_r \approx 0.1$ (e.g., Panaitescu et al. 1999; Kumar 1999) to $f_r \approx 1$ (e.g., Beloborodov 2000) of the energy dynamically converted into thermal or magnetic energy. Thus, the radiative efficiency of the process, measured as the fraction of the total initial energy converted into radiation, will be $1/f_r$ times smaller than the computed dynamic efficiency. Even considering this factor, single binary collisions between moderately magnetized shells may yield efficiencies $\sim 0.4f_r$, which can obviously rise if many binary collisions take place in the flow reprocessing the remaining kinetic energy of the first generation of interacting shells (in the same statistical way as discussed by Kobayashi & Sari 2000). Therefore, on the light of our results, binary collisions in relativistic magnetized flows are efficient enough, from the dynamical point of view, to be a valid mechanism to dissipate the bulk kinetic energy of relativistic ejecta. Hence, the main restriction on the radiative efficiency comes from the radiation mechanism setting the limiting factor f_r .

We stress that we are not assuming any particular radiation mechanism in this study (thus, determining a value for f_r). Therefore, we compute the dynamic efficiency including not only the increased thermal energy in the flow, but also the extra magnetic energy resulting from the magnetic field compression. This is justified because, although standard shock acceleration mechanisms are inefficient in very magnetized shocks (e.g., Sironi & Spitkovsky 2009), other mechanisms might extract the energy from the whole volume of a very magnetized fluid (e.g., Thompson 1994; Giannios & Spruit 2007).

The estimated dynamic efficiency in the binary collision of magnetized shells will be completed in a future work by accounting for the numerical MHD evolution of such building blocks of the internal shock models. A step further would be to compute the radiative efficiency using the method devised in Mimica et al. (2009).

ACKNOWLEDGMENTS

MAA is a Ramón y Cajal Fellow of the Spanish Ministry of Education and Science. We acknowledge the support from the Spanish Ministry of Education and Science through grants AYA2007-67626-C03-01 and CSD2007-00050. We thank José-María Martí and José-María Ibáñez for their support and critical discussions. The authors thankfully acknowledge the computer resources, technical expertise and assistance provided by the Barcelona Supercomputing Center - Centro Nacional de Supercomputación.

APPENDIX A: EQUATION OF STATE

In this Appendix we discuss the effects of using a more realistic equation of state on our results. We choose the *TM* analytic approximation to the Sygne equation of state (EoS) (de Berredo-Peixoto et al. 2005; Mignone et al. 2005). In the *TM* EoS the specific enthalpy can be written as (using the notation of Section 2.1)

$$h_{TM}^* := \frac{5}{2} \frac{p^*}{\rho} - \frac{\sigma}{4} + \left[\frac{9}{4} \left(\frac{p^*}{\rho} - \frac{\sigma}{2} \right)^2 + 1 \right]^{1/2}. \quad (\text{A1})$$

and the specific internal energy

$$\epsilon_{TM} := \frac{3}{2} \frac{p}{\rho} + \left[\frac{9}{4} \left(\frac{p}{\rho} \right)^2 + 1 \right]^{1/2} - 1. \quad (\text{A2})$$

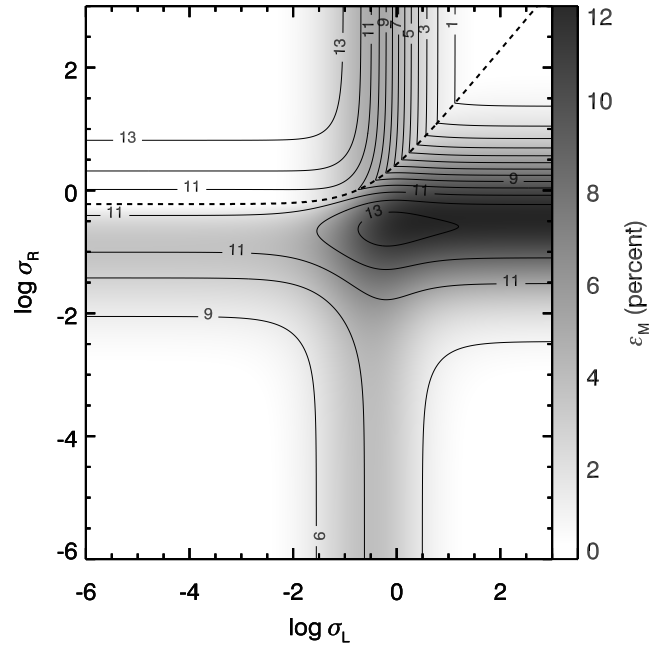


Figure A1. Same as Fig. 2, but for the *TM* equation of state.

From (A1) it can be seen that the limit $\sigma = 0$ the effective adiabatic index of this EoS lies between $4/3$ and $5/3$. We modified the Romero et al. (2005) solver to include the *TM* EoS.

On Fig. A1 we show the dynamical efficiency in the GRB regime using the *TM* EoS. Comparison of Fig. 2 and Fig. A1 shows that, overall, the dynamical efficiency is higher when using the *TM* EoS, but the qualitative features remain the same in both cases. Also, as expected, in the highly magnetized regime the differences are minor, since in both cases (polytropic or *TM* EoS) the effective adiabatic index approaches 2 in such a regime. Figure A2 shows the influence of the EoS on the existence of the FS. The only difference between models with different EoS appears in the region where the faster shell is weakly magnetized. There a slightly higher (lower) magnetization of the slower shell is needed to suppress the FS when using *TM* than when using a polytropic EoS with $\hat{\gamma} = 4/3$ ($\hat{\gamma} = 5/3$). The overlap of all three curves in Fig. A2 in the limit of high magnetization of both shells, shows again the result that the choice of EoS plays no role in such a regime, as expected. We note that the separatrix between the regions of existence and non-existence of the FS corresponding to the case $\hat{\gamma} = 5/3$ lies closer to that of the *TM* EoS than that corresponding to the case $\hat{\gamma} = 4/3$. This is a natural consequence of the fact that the initial shells are both cold, and thus, the effective adiabatic index is closer to $5/3$ than to $4/3$, at low magnetizations.

We note that in the case of the external shocks, where relativistic fluid encounters a cold external medium the choice of the realistic EoS can influence results much more dramatically than in the case of the internal shocks (see e.g., Meliani et al. 2008).

REFERENCES

- Aloy M. A., Janka H.-T., Müller E., 2005, *A&A*, 436, 273
- Aloy M. A., Mimica P., 2008, *ApJ*, 681, 84
- Aloy M. A., Müller E., Ibáñez J. M., Martí J., MacFadyen A., 2000, *ApJL*, 531, L119
- Aloy M. A., Rezzolla L., 2006, *ApJ*, 640, L115

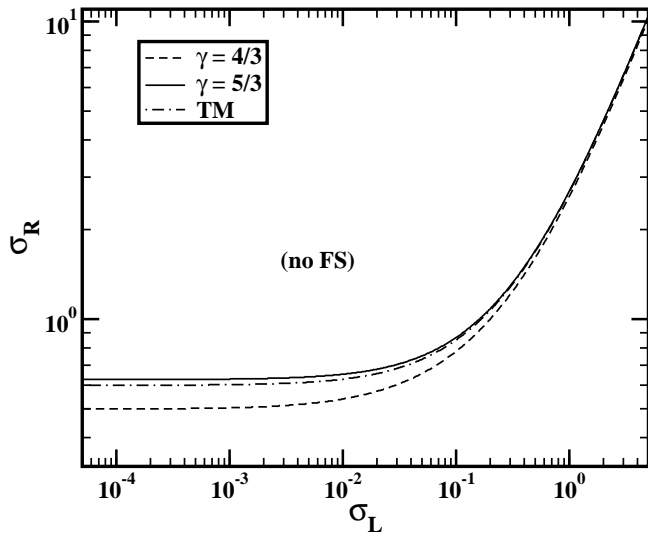


Figure A2. Comparison of the separatrix lines dividing regions of existence and non-existence of the forward shock (located above each line, the region where the forward shock is not formed). Solid and dashed lines correspond to the polytropic EoS with $\hat{\gamma} = 5/3$ and $\hat{\gamma} = 4/3$, respectively, while the dot-dashed line shows result for the *TM* EoS.

Beloborodov A. M., 2000, *ApJ*, 539, L25
 Bošnjak Ž., Daigne F., Dubus G., 2009, *A&A*, 498, 677
 Daigne F., Mochkovitch R., 1998, *MNRAS*, 296, 275
 de Berredo-Peixoto G., Shapiro I. L., Sobreira F., 2005, *Modern Physics Letters A*, 20, 2723
 Fan Y., Piran T., 2006, *MNRAS*, 369, 197
 Fan Y. Z., Wei D. M., Zhang B., 2004, *MNRAS*, 354, 1031
 Giacomazzo B., Rezzolla L., 2006, *Journal of Fluid Mechanics*, 562, 223
 Giannios D., Spruit H. C., 2007, *A&A*, 469, 1
 Kennel C. F., Coroniti F. V., 1984, *ApJ*, 283, 694
 Kino M., Mizuta A., Yamada S., 2004, *ApJ*, 611, 1021
 Kino M., Takahara F., 2008, *MNRAS*, 383, 713
 Kobayashi S., Piran T., Sari R., 1997, *ApJ*, 490, 92
 Kobayashi S., Ryde F., MacFadyen A., 2002, *ApJ*, 577, 302
 Kobayashi S., Sari R., 2000, *ApJ*, 542, 819
 Kobayashi S., Sari R., 2001, *ApJ*, 551, 934
 Kumar P., 1999, *ApJ*, 523, L113
 Lazzati D., Ghisellini G., Celotti A., 1999, *MNRAS*, 309, L13
 Lazzati D., Morsony B. J., Begelman M. C., 2009, *ApJL*, 700, L47
 Leisemann T., Antón L., Aloy M. A., Müller E., Martí J., Miralles J. A., Ibáñez J. M., 2005, *A&A*, 436, 503
 Meliani Z., Keppens R., Giacomazzo B., 2008, *A&A*, 491, 321
 Mignone A., Plewa T., Bodo G., 2005, *ApJS*, 160, 199
 Mimica P., Aloy M.-A., Agudo I., Martí J. M., Gómez J. L., Miralles J. A., 2009, *ApJ*, 696, 1142
 Mimica P., Aloy M. A., Müller E., 2007, *A&A*, 466, 93
 Mimica P., Aloy M. A., Müller E., Brinkmann W., 2004, *A&A*, 418, 947
 Mimica P., Aloy M. A., Müller E., Brinkmann W., 2005, *A&A*, 441, 103
 Mimica P., Giannios D., Aloy M. A., 2009, *A&A*, 494, 879
 Mizuta A., Aloy M. A., 2009, *ApJ*, 699, 1261
 Mizuta A., Yamasaki T., Nagataki S., Mineshige S., 2006, *ApJ*, 651, 960
 Morsony B. J., Lazzati D., Begelman M. C., 2007, *ApJ*, 665, 569

Nakar E., Piran T., 2002, *ApJ*, 572, L139
 Panaitescu A., Spada M., Mészáros P., 1999, *ApJ*, 522, L105
 Piran T., 2005, *Reviews of Modern Physics*, 76, 1143
 Rees M. J., Gunn J. E., 1974, *MNRAS*, 167, 1
 Rees M. J., Meszaros P., 1994, *ApJL*, 430, L93
 Rezzolla L., Zanotti O., 2001, *Journal of Fluid Mechanics*, 449, 395
 Romero R., Martí J., Pons J. A., Ibáñez J. M., Miralles J. A., 2005, *Journal of Fluid Mechanics*, 544, 323
 Sari R., Piran T., 1995, *ApJL*, 455, L143
 Sari R., Piran T., 1997, *ApJ*, 485, 270
 Sironi L., Spitkovsky A., 2009, *ApJ*, 698, 1523
 Spada M., Ghisellini G., Lazzati D., Celotti A., 2001, *MNRAS*, 325, 1559
 Tanihata C., Takahashi T., Kataoka J., Madejski G. M., 2003, *ApJ*, 584, 153
 Thompson C., 1994, *MNRAS*, 270, 480
 Usov V. V., 1992, *Nature*, 357, 472
 van der Holst B., Keppens R., Meliani Z., 2008, *Computer Physics Communications*, 179, 617
 Zhang B., Mészáros P., 2004, *International Journal of Modern Physics A*, 19, 2385
 Zhang W., Woosley S. E., Heger A., 2004, *ApJ*, 608, 365
 Zhang W., Woosley S. E., MacFadyen A. I., 2003, *ApJ*, 586, 356